

Robotics-driven Printing of Curved 3D Structures for Manufacturing Cardiac Therapeutic Devices

Zeyu Wang^{1,2}, James K. Min², and Guanglei Xiong²

1200012927@pku.edu.cn, jkm2001@med.cornell.edu, gux2003@med.cornell.edu

Abstract—Cardiovascular disease (CVD) is the leading cause of death in the United States. 3D printing technology has increasingly paved its way into cardiovascular applications, in particular for manufacturing cardiac therapeutic devices. However, currently available commercial 3D printers and those under development exclusively work by successively depositing layers of material using axis-aligned slicing methods, thus need unacceptably high demand of support materials and even fail fabricating for some complex cardiovascular structures, not to mention printing for the purpose of repairing an existing abnormal strictures. To solve this problem, we propose and develop a novel and robust robotics-driven printing system, consisting of a robotic arm and an extruder tool to allow printing along trajectories on any curved surface. Given the target structure, a new set of algorithms for robot toolpath planning was implemented, which include mesh parameterization, distance transform, contouring and smooth interpolation. Using both simulation and actual physical testing, we showed our system can successfully print layers of the target structure on curved geometry by following planned tool paths and depositing materials. In this paper, we describe our methodology and algorithm pipeline, compare and analyze the printing results of different techniques, and most importantly, envision the promising future extension of our robotics-driven printing system in manufacturing cardiac therapeutic devices.

I. INTRODUCTION

Cardiovascular disease is the leading cause of death for both men and women in the United States [1]. The mortality and mobility rates related to CVD have been greatly reduced, due to continuous advances in therapeutic devices and surgical procedures, such as transcatheter aortic valve replacement, coronary bypass graft, and total artificial heart replacement [2]. A major challenge that affects the field of cardiovascular surgery is the shortage of devices that match the performance of autologous or heterologous tissue available for surgical reconstructive procedures. In addition, thrombosis, infections and rejection of the foreign devices by the host often complicate surgical outcomes. Biomedical engineering of new therapeutic devices has become one of the frontiers in cardiovascular surgery to address these issues [3], by providing the ability to seed devices using the patient's own cells in synthetic biomimetic supporting scaffolds. To support cell adhesion and neotissue formation, scaffolds need to provide an internal environment that closely resembles native extracellular matrix (ECM), in terms of both structure and function, since the internal architecture of ECM

greatly influences crucial factors for tissue regeneration, such as nutrient diffusion and permeability, cell adhesion and signaling [4]. Furthermore, scaffolds should maintain a sufficient level of structural stability and durability to withstand external stresses and stimuli. However, conventional techniques such as molding or electrospinning cannot create scaffolds of sufficient heterogeneity of the internal structure and flexible mechanical properties, as those seen in native tissues [5].

To date, 3D printing has shown great promise in manufacturing next-generation therapeutic devices for cardiovascular surgery, which often involves complicated 3D scaffolding structures. However, limited success was reported to fabricate scaffolds using biocompatible and biodegradable polymers (e.g. hydrogel) for prototyping preclinical devices, such as myocardial patches, heart valves and microvasculature. For example, Gaetani et al. [6] used a 3D printer to generate a porous gel-based scaffold containing human cardiac-derived cardiomyocyte progenitor cells (hCMPCs) and tested how different porosities affect viability of hCMPCs. Hockaday et al. [7] developed an extrusion-based 3D printer to deposit two types of ultraviolet (UV) curable hydrogels, one stiff for the aortic root and the other soft one for the valve leaflets. They also showed that porcine aortic valve interstitial cells could be seeded into the printed heart valves and survive for up to three weeks. Miller et al. [8] printed rigid 3D filament networks of sacrificial material based on carbohydrates for rapid casting of patterned vascular networks in engineered tissues using extrusion through a syringe mounted on a modified 3D printer. To show the flexibility of the approach, they patterned vascular channels in the presence of living cells and observed three key compartments of vascularized solid tissues. Despite these promising results, 3D printed scaffolding structures have not matched the requirements of manufacturing device or replacement tissue constructs for clinical uses.

The overall scheme of 3D printing adopted in all open and commercial platforms is typically to first convert the desired object into layers of 2D slices and then deposit materials sequentially in a layer-by-layer fashion [9]. When this method is used to form large structures of complex curved shapes, as they occur in natural cardiac tissues and blood vessels, three fundamental issues exist. The first issue is the necessity of adding and removing support material to prevent overhanging features from collapsing into subsequent layers. This strategy, however, requires the printing of an additional material, which is sacrificial, and therefore requires

¹Key Laboratory of Machine Perception, School of Electronics Engineering and Computer Science, Peking University, Beijing, 100871, China.

²Dalio Institute of Cardiovascular Imaging, Weill Cornell Medical College, Cornell University, New York, NY 10021, USA.

additional post-processing that can either be time-consuming or even impossible without damages, for example, long and curved vascular grafts with small openings and soft materials. Furthermore, thin-walled shell structures of high curvature are also difficult to fabricate since the printer head is only directed to move within a 2D plane and formation of the shell requires printing small pieces in many slices, which leads to serious artifacts of discretization. The last issue is the constraint of aligning internal structures to a Cartesian grid. Thus, it is impossible to create scaffolds mimicking curvilinear fiber orientations observed in all cardiovascular tissues so far. To overcome these problems, we propose to develop a new 3D printing system that utilizes a fluid dispensing nozzle mounted on a robotic arm. Our system is especially designed to fabricate curved scaffolds of any internal structure without supports.

II. METHODOLOGY

A. Overview and Preparation

Fig. 1 shows the design of our robotics-driven 3D printer. The system utilizes an industrial robotic arm (ABB IRB 120) with 6 degrees of freedom. The end effector of the robotic arm is loaded with a dispensing syringe. The nozzle deposits UV curable materials when moving in the pre-calculated trajectory, as guided by the robotic arm. The dispense rate at the nozzle is driven by a pneumatic pressure source. Therefore, an additional support material is completely unnecessary in our system, negating the need for a post-processing step. The robotic arm and the fluidic pump are precisely controlled and synchronized with a central control system on a computer. Due to the arbitrary trajectories of our robotic arm, our system is not only capable of building a 3D scaffold on a flat surface from scratch, but also thin-walled curved scaffolds on a curved surface of a pre-existing object.

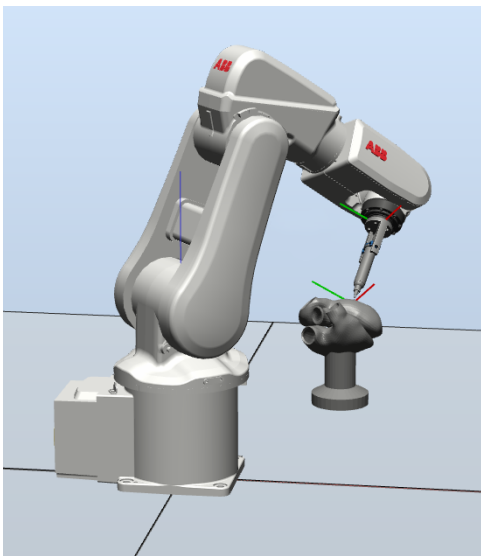


Fig. 1. Robotic arm prints target model on the pre-existing object using dispensing syringe.

To prepare the object, we first design a mesh model of

human heart with four chambers, and load it on a commercial 3D printer (Stratasys Objet260 Connex), which takes the aforementioned layer-by-layer strategy. After almost 12-hour printing process, we have the object buried in massive support materials, as shown in the left of Fig. 2. The right one is the actual expected model whose support materials are carefully removed using delicate shovels and high pressure water jets.



Fig. 2. Newly printed object (left) and after post-processing, which is used as the pre-existing model.

Fig. 3 depicts the pipeline of computer algorithms, which is developed for our new robotics-based printing system. Depending on the source of inputs from medical imaging data or computer-aided design tools, the scaffold geometry can either be a triangular/quadrilateral mesh or a NURBS-based boundary representation. We first convert the input geometry into a triangular surface mesh. In the geometry preparation step, the input mesh is scanned for common errors of non-manifold features (such as holes, flipped triangles) and refined (decimation, hole filling, smoothing, etc.) to create a water-tight mesh with good-quality triangles. To fill the internal void with fiber structures, we develop an algorithm that can be operated either in a fully-automated or user-guided fashion. The central idea is to design curvilinear space filling curves using vector fields specified on the external surface. There are three steps:

- 1) A vector field is automatically designed based on positioning of singularities and refined by user-defined preferred directions;
- 2) Tubular fiber structures are formed by generating streamline curves, which follows the designed vector field. The radius of the fiber may be spatially varied, by changing the extrusion rate;
- 3) The vector fields and streamlines are propagated into the internal space by distance transform using the fast marching method.

B. Mesh Parameterization

Once we have the pre-existing object and a target scaffold shape, whose representation is preprocessed into a triangular mesh, our primary objective is to find a traversing solution in this region. Instead of naive scanning lines, which dominates

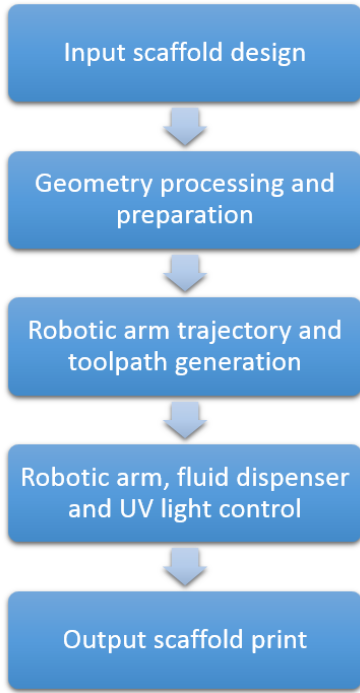


Fig. 3. System pipeline of computer algorithms.

current layer-by-layer 3D printers, a more robust method is proposed adopting contours. In order to achieve this, we first do mesh parameterization, aiming to find a bijective mapping from the triangular mesh onto a parameter domain. Here we use the definition of a popular parameter domain in computer graphics, on which further algorithms will take place.

Suppose that $\Omega \subset \mathbb{R}^2$ is some simply connected region (i.e., without any holes), for example the unit square,

$$\Omega = \{(u, v) \in \mathbb{R}^2 : u, v \in [0, 1]\} \quad (1)$$

and that the function $f : \Omega \rightarrow \mathbb{R}^3$ is continuous and an injection (i.e., no two distinct points in Ω are mapped to the same point in \mathbb{R}^3). We then call the image S of Ω under f a surface,

$$S = f(\Omega) = \{f(u, v) : (u, v) \in \Omega\} \quad (2)$$

and say that f is a parameterization of S over the parameter domain Ω . It follows from the definition of S that f is actually a bijection between Ω and S and thus admits to define its inverse $f^{-1} : S \rightarrow \Omega$ [10].

There are various methods solving this problem. Some minimize distortion according to angles, while others minimize distortion according to distances or areas. Some have fixed and convex boundary, while others have free boundary. Some are not bijective, while others are bijective locally or globally. In addition, their complexity varies as well [11]. We use the Least Squares Conformal Mapping (LSCM) method implemented in the Open-Source Blender modeler [12]. Fig. 4 shows the result.

C. Distance Transform

Mesh parameterization provides a planar representation of the scaffold. Intuitively, it is a good choice to print along the contours from outside to inside, and distance transform is an important step to make it happen. In image processing, distance transform, also known as grassfire transform, is the computation of distance from a pixel to the border of a region. There are several distance metrics, including Euclidean, which is most suitable for our algorithm, city block, chessboard, quasi-Euclidean, etc. In MATLAB, the `bwdist` function can calculate distance transform for binary images using fast algorithm [13], as shown in the left of Fig. 5.

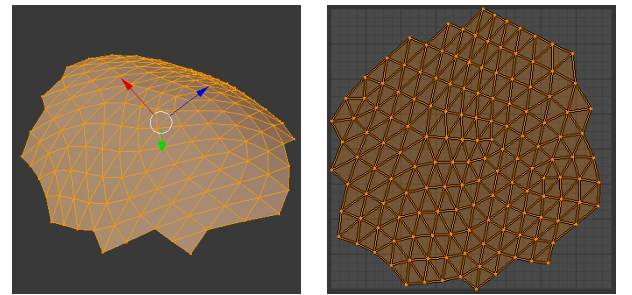


Fig. 4. Sample scaffold mesh (left) and its parameterization.

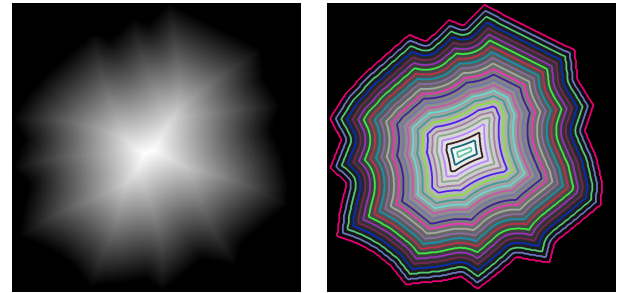


Fig. 5. Distance transform (left) and contour marching.

D. Contour Marching

The result of distance transform implies the chronological order when syringe is extruding and printing. Considering the materials have some breadth, this task can be accomplished traversing isocontours of different level from outside to inside. To generate the isocontour toolpath in the scalar field, marching squares algorithm is needed. It takes a similar approach to the 3D marching cubes algorithm, which contains following four steps [14]:

- 1) Process and label each cell in the grid independently, according to the given threshold;
- 2) Calculate a cell index using comparisons of the contour levels with the data values at the cell corners;
- 3) Use a pre-built lookup table (Fig. 6), keyed on the cell index, to describe the output geometry for the cell;
- 4) Apply linear interpolation along the boundaries of the cell to calculate the exact contour position.

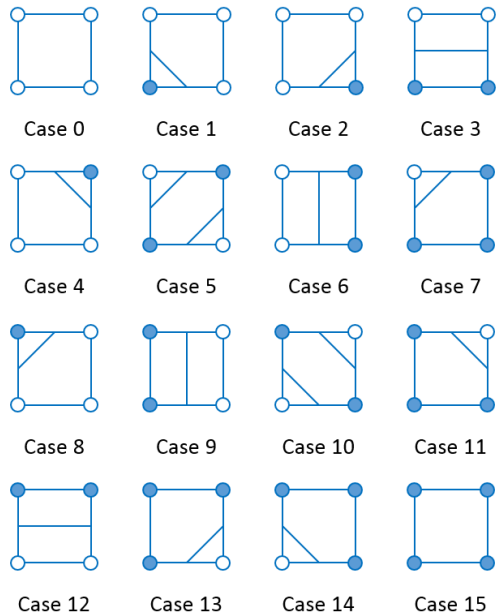


Fig. 6. Pre-built lookup table for marching squares.

E. Printer Control

For control of the printer, fast algorithms are developed to convert the planned trajectories of the robotic arm into real-time instructions to the robots. To begin with, marching squares provide the position of contour nodes in parameter domain, from which we can locate the indices of triangle that they belong to. Mesh vertices have known spatial coordinates and corresponding information in parameter domain. Thus, using barycentric interpolation, we can get the spatial coordinates of arbitrary contour nodes. Except for translation, rotation has three more degrees of freedom that we should also concern. To avoid collision, we set the nozzle at a parallel direction to the normal of current position. In the first place, vertex normals are calculated as the weighted average of normals of all its adjacent faces. Then, the normal of any arbitrary position can be calculated similarly using barycentric interpolation. Translation and rotation form all the information of robotic arm toolpath.

There is another issue. What we have got so far are totally based on the coordinate system of scaffold model. When the pre-existing object is put into the configuration space of robotic arm, a transformation for calibration is mandatory, which we can effectively represent with a quaternion. The calibrated trajectories are converted through inverse kinematics by the configuration of the robotic arm. We also put limitations on the velocities and accelerations to avoid irregular and uneven tracing of the material.

As for fluid dispenser control and UV curing light control, the pressure of the fluid dispensing for syringe nozzle is modulated to control the speed of the materials being deposited or shut off when the nozzle is not on the intended trajectory, especially when moving between previous contour and current contour. It can also stay accordance with the

moving speed of syringe by adjusting sampling rate of nodes and robotic arm settings. In addition, the UV curing light is synchronized with whether material is being extruded, thus guarantee that the materials are cured promptly and the nozzle would not be blocked as well.

III. RESULTS AND ANALYSIS

A. Experiments

Our experimental environment includes a robotic arm (ABB IRB 120), a mounted syringe (Nordson EFD Optimum 100cc) filled with silicone (Momentive Performance Materials Inc.), an air pressure controller (Nordson EFD Ultimus V) and a UV lamp (Smith-Vector Corporation), as shown in Fig. 7.

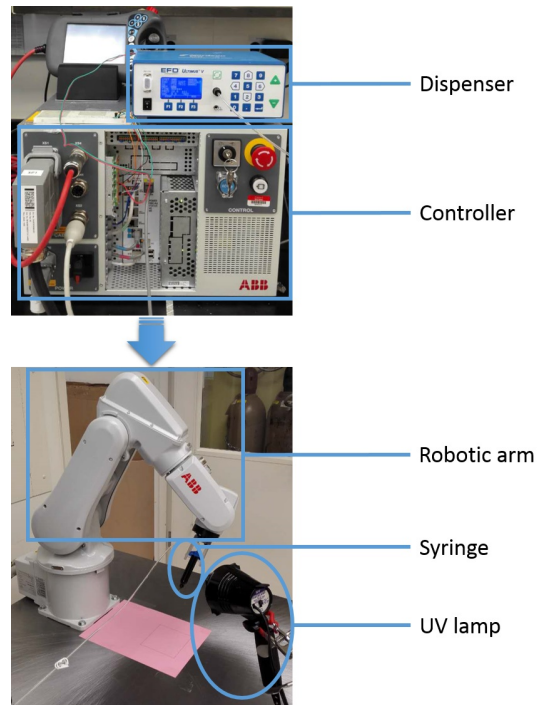


Fig. 7. Experimental environment overview.

The first thing that we should do is calibration. For simplicity, our heart model is put on the $z = 0$ surface with a square pedestal, with an edge length of 100mm and the center on $(300, 0, 0)$. Thus we can manipulate the robotic arm to touch these four points, i.e. $(250, 50, 0)$, $(350, 50, 0)$, $(350, -50, 0)$, $(250, -50, 0)$, and then mark labels. Once we fix the pre-existing model and finish the calibration, the coordinate system in RobotStudio stays accordance with the real setup.

In the next step, we filled the syringe with silicone and test program on the robotic arm. The moving speed can be adjust both in RobotStudio and changing the sampling rate of data. The velocity of flow depends on the air pressure of dispenser and the diameter of nozzle. Considering that our main approach adopts contours rather than scanning lines, the number of rounds is also a parameter that we can adjust, which is directly related to the step length of contour

marching on the transformed distance map. The exposure time to UV light decides the curing level of silicone. The longer it is, the more stable and solidified the silicone is. Table I summarizes all the factors that may have an influence on our printing effect, as well as several case settings that we test.

TABLE I
FACTORS THAT MAY AFFECT PRINTING RESULTS

#Case	A	B	C
Air pressure / kPa	20	10	10
Step length / brightness	0.10	0.10	0.05
Exposure time / second	60	60	60

B. Analysis

Currently, we printed a surface instead of a shape. To evaluate the difference between our printed surface and the designed model, it is a good choice to use image analysis techniques. With the position of a camera fixed, we take several pictures of each printed result. Hausdorff distance is an effective and widely used metric for simple contour measurement [15], with the following definition. Intuitively, it finds the point x from the set X that is farthest from any point in Y and measures the distance from x to its nearest neighbor in Y , and vice versa.

$$d_H(X, Y) = \max \left\{ \sup_{x \in X} \inf_{y \in Y} d(x, y), \sup_{y \in Y} \inf_{x \in X} d(x, y) \right\} \quad (3)$$

As for parameters, it is assumed that the brightness of the brightest part in the transformed distance map is 1, and that of the darkest part is 0. For traversing the target surface, the step length of 0.05 and 0.10 are selected, with the corresponding number of rounds of 20 and 10 respectively. Moreover, the extrusion rate of silicone is decided by air pressure, which we set to 10kPa and 20kPa for comparison.

In order to take advantage of this measurement, preprocessing is required. Given the pictures, we first calculate intensity gradients both horizontally and vertically, and add their absolute value together to detect edges. Through intensity remapping and thresholding methods, noise can be eliminated in a judicious manner. Then we extract the clean data of surface trajectories, which can be set as input of Hausdorff distance analysis module. The similarity between our results and ground truth is listed in Table II.

$$G(I) = \left| \frac{\partial}{\partial x} I \right| + \left| \frac{\partial}{\partial y} I \right| \quad (4)$$

TABLE II
HAUSDORFF DISTANCE AMONG THREE RESULTS

#Case	A	B	C
A	-	62.2254	72.8354
B	62.2254	-	47.3814
C	72.8354	47.3814	-

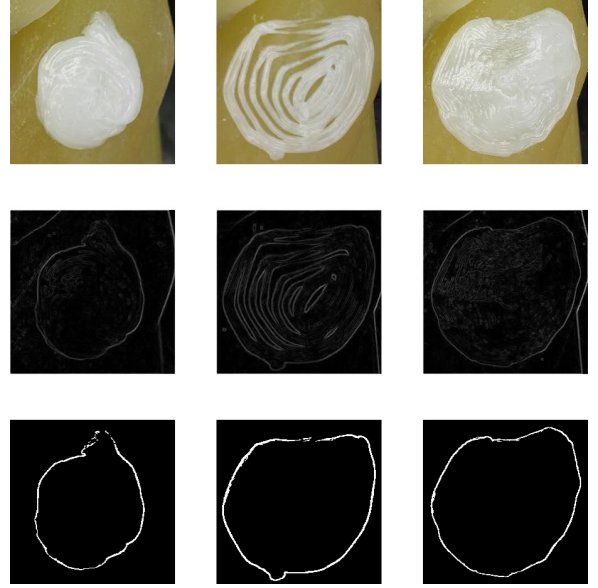


Fig. 8. Contour analysis of three cases.

From the images and calculation above we can see that the best printing effect comes with the step length of 0.05, i.e. 20 traversing rounds. This result tells us that to avoid gaps and over-dispensation, the number of rounds can be neither too large nor too small, and that it has to keep consistent with the settings of air pressure and nozzle diameter. Except for contour analysis, here are some preliminary analyses of appearance and material. In this case, we use silicone because it is originally liquid and can be cured to solid state using UV light. By comparison with VeroClear, a popular material in many commercial 3D printers, cured silicone is also translucent, but softer, which provides the possibility of medical and clinical applications.

Last but not least, it is a wise decision to have more insights into these algorithms. Here we mainly use three algorithms, mesh parameterization, distance transform and marching squares. For the complexity, we first define N as the size of vertices on target mesh, and M as the resolution of transformed distance map. Fortunately, the LSCM method for mesh parameterization and Calvin's algorithm for Euclidean distance transform both have linear complexity [11][13]. In the stage of contour marching, we match each pixel to sixteen cases in the pre-built lookup table, thus its complexity is also linear. In summary, the total time complexity of our system is $O(N + M)$, and can be regarded as $O(M)$ since the resolution is much greater than the size of vertices in most instances.

In the future, we will print multilayer shapes along the surface of pre-existing model. Each layer is the intersection part of designed target shape and model's expanded surface along their normal directions. To evaluate this, we will adopt 3D scanners to obtain the actual model of our printing results. After mesh reconstruction from point clouds, analysis on 3D scale will appraise the performance of our system more accurately, and will offer feedbacks for potential improvement.

IV. CONCLUSION AND FUTURE WORK

To date, no prior 3D printer has been built to directly fabricate curved scaffold geometries without the need of support materials. However, we believe the capability to fabricate this kind of structure will make an important transition from 2D flat bioengineered devices to a more curved and heterogeneous form, as seen in the native tissues. To eliminate the limitations of common 3D printer schemes, which use layer-by-layer deposition, we propose to build a robotics-based 3D printer that allows fabricating curved scaffold geometries flexibly, and without support structures. With the ability to deposit a range of UV curable materials, such as hydrogels, the printer will make a great impact in research and development of cardiovascular biomedical engineering for next-generation therapeutic devices.

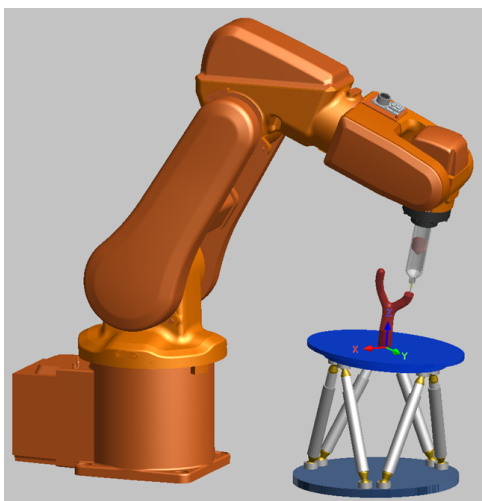


Fig. 9. A possible prospect of our future system.

Our robotics-based 3D printer is much more advanced compared with computer numerical control (CNC) machines and common 3D printers. In addition, a rotary moving table, such as the Hexapod Stewart platform can be also set up to introduce more degrees of freedom and to improve reachability, thus to satisfy the requirement of various shapes. The printed sample should be placed on the table, driven by six prismatic actuators. The table is rapidly tilted to ensure the deposited material is supported sufficiently by surface tension and not overcome by gravity. For the toolpath generation, the pose (i.e. translation and rotation) of the moving table is changed whenever an overhanging feature is detected in the fiber structure, which can be realized by a mounted camera using computer vision techniques. Traversing each fiber, the pose of the table should be modified to eliminate the potential overhang (no material deposited beneath it), which has extrusion larger than the critical angle (e.g. 30°) of the cured material. The new pose of the table is determined by maximizing the length of overhang-free trajectory until the next overhang, and the consecutive poses of robotic arm and its nozzle can be calibrated correspondingly from planned trajectory by the stored transformation matrix.

From the perspective of algorithm, currently we convert 3D to 2D just in order to do path planning, and then interpolate the coordinates to generate trajectory. Theoretically, some uniformity will be lost if curvature of surfaces is not taken into consideration. In the future, we will investigate and implement geodesic distance transform to avoid 3D-to-2D converting as well as to promote consistency and robustness. A possible prospect of our future system is shown in Fig. 9.

ACKNOWLEDGMENT

This work was supported by the national center for advancing translational science of the national institute of health under award number UL1TR000457. We would like to thank Dr. Dirk-Jan Kroon and Dr. Zachary Danziger for contributing `isocontour` and `HausdorffDist` function.

REFERENCES

- [1] Sherry L Murphy, Jiaquan Xu, and Kenneth D Kochanek. Deaths: final data for 2010. *National vital statistics reports: from the Centers for Disease Control and Prevention, National Center for Health Statistics, National Vital Statistics System*, 61(4):1–117, 2013.
- [2] Alan S Go, Dariush Mozaffarian, Véronique L Roger, Emelia J Benjamin, Jarett D Berry, Michael J Blaha, Shifan Dai, Earl S Ford, Caroline S Fox, Sheila Franco, et al. Heart disease and stroke statistics—2014 update: a report from the american heart association. *Circulation*, 129(3):e28, 2014.
- [3] Marc N Hirt, Arne Hansen, and Thomas Eschenhagen. Cardiac tissue engineering state of the art. *Circulation research*, 114(2):354–367, 2014.
- [4] Scott J Hollister. Porous scaffold design for tissue engineering. *Nature materials*, 4(7):518–524, 2005.
- [5] Ulrich Boudriot, Roland Dersch, Andreas Greiner, and Joachim H Wendorff. Electrospinning approaches toward scaffold engineering: a brief overview. *Artificial organs*, 30(10):785–792, 2006.
- [6] Roberto Gaetani, Peter A Doevendans, Corina HG Metz, Jacqueline Alblas, Elisa Messina, Alessandro Giacomello, and Joost PG Sluijter. Cardiac tissue engineering using tissue printing technology and human cardiac progenitor cells. *Biomaterials*, 33(6):1782–1790, 2012.
- [7] LA Hockaday, KH Kang, NW Colangelo, PYC Cheung, B Duan, E Malone, J Wu, LN Girardi, LJ Bonassar, H Lipson, et al. Rapid 3d printing of anatomically accurate and mechanically heterogeneous aortic valve hydrogel scaffolds. *Biofabrication*, 4(3):035005, 2012.
- [8] Jordan S Miller, Kelly R Stevens, Michael T Yang, Brendon M Baker, Duc-Huy T Nguyen, Daniel M Cohen, Esteban Toro, Alice A Chen, Peter A Galic, Xiang Yu, et al. Rapid casting of patterned vascular networks for perfusable engineered three-dimensional tissues. *Nature materials*, 11(9):768–774, 2012.
- [9] D Dimitrov, K Schreive, and N De Beer. Advances in three dimensional printing-state of the art and future perspectives. *Journal for New Generation Sciences*, 4(1):p–21, 2006.
- [10] Alla Sheffer, K Hormann, B Levy, M Desbrun, K Zhou, E PRAUN, and H HOPPE. Mesh parameterization: Theory and practice. *ACM SIGGRAPH, course notes*, 2007.
- [11] Alla Sheffer, Emil Praun, and Kenneth Rose. Mesh parameterization methods and their applications. *Foundations and Trends® in Computer Graphics and Vision*, 2(2):105–171, 2006.
- [12] Bruno Lévy, Sylvain Petitjean, Nicolas Ray, and Jérôme Maillot. Least squares conformal maps for automatic texture atlas generation. In *ACM Transactions on Graphics (TOG)*, volume 21, pages 362–371. ACM, 2002.
- [13] Calvin R Maurer Jr, Rensheng Qi, and Vijay Raghavan. A linear time algorithm for computing exact euclidean distance transforms of binary images in arbitrary dimensions. *Pattern Analysis and Machine Intelligence, IEEE Transactions on*, 25(2):265–270, 2003.
- [14] William E Lorensen and Harvey E Cline. Marching cubes: A high resolution 3d surface construction algorithm. In *ACM siggraph computer graphics*, volume 21, pages 163–169. ACM, 1987.
- [15] Daniel P Huttenlocher, Gregory Klanderman, William J Rucklidge, et al. Comparing images using the hausdorff distance. *Pattern Analysis and Machine Intelligence, IEEE Transactions on*, 15(9):850–863, 1993.